A simple, robust, and automatic approach to extract water body from Landsat images (case study: Lake Urmia, Iran)

Hadiseh Babaei, Milad Janalipour and Nadia Abbaszadeh Tehrani

ABSTRACT

Lake Urmia is one of the largest saline lakes in the world, and has a great effect on its surrounding ecosystems as well as the economic, social, and even cultural condition of its basin inhabitants. Hence, continuous monitoring of lake area changes is necessary and unavoidable for better land management and prevention of its degradation. In this study, by using Landsat 8 images and by preforming some essential pre-processing tasks, the area of the lake was estimated using the number of traditional spectral indices and a new one and the automatic Otsu's thresholding method for 5 years (2013–2017). The results showed that this index shows more accurate results than other indices when estimating the area of the lake and can separate water class from land one with an average overall accuracy of 96%.

Key words | Landsat, Otsu's thresholding method, remote sensing, saline lake, spectral indices, WSSI

Hadiseh Babaei
Milad Janalipour (corresponding author)
Nadia Abbaszadeh Tehrani
Aerospace Research Institute, Ministry of Science, Research and Technology,
Tehran,
Iran
E-mail: *m_janalipour89@yahoo.com*; *milad_janalipour@ari.ac.ir*

INTRODUCTION

Lake Urmia is considered an important aquatic ecosystem in Iran, with approximately 550 plant species recorded to be growing in its ecological area. It was introduced as a biosphere reserve by the United Nations Educational, Scientific and Cultural Organization (UNESCO) since 1976 and recognized as a home to a number of migrating waterfowl in winter (Maleki *et al.* 2018). Continuous monitoring of its water-level fluctuations and the drying procedure is very important for future studies. In the late 1990s, Lake Urmia was the largest salt lake in the Middle East, but its area reduced significantly over time, so that it had reduced by half in 2008 and one-fifth in 2015. This area reduction has many environmental impacts, such as increasing salinity level of the lake and the extinction of a salinity-resistant shrimp named Artemia (Abatzopoulos *et al.* 2006; Eimanifar & Mohebbi 2007).

In recent years, many studies in the Urmia Lake basin and other water bodies around the world were done in order to monitor their behavior using remote sensing (Huovinen *et al.* 2019; Mohebzadeh & Fallah 2019). In most of these studies, the lake expansion or its water area was determined using spectral indices or different classification methods. In order to extract water body from the spectral indices, a threshold value based on a trial-and-error was chosen to classify water body and land (Xu 2006; Feyisa *et al.* 2014). Selecting an optimized threshold value in a trial-and-error manner is time-consuming. Therefore, examining the possibility of using automated thresholding methods helps us to save time and improves the accuracy of results. Most of the time, the threshold is a constant value that works well, but it may be challenging to select its appropriate value in case of shades, hills, forest, and urban areas (Acharya *et al.* 2017). In most studies, the threshold value of 0 was considered for water indices, but researches have shown that adjustment of this threshold for each region will increase the accuracy of water extraction. Adjusting the threshold value is very difficult, especially when time-series images are used for the same water body; therefore, some studies attempted to select the threshold value in an automatic manner (Huang *et al.* 2018). Li & Sheng (2012) developed a new automated method based on the

doi: 10.2166/wcc.2019.078

Normalized Difference Water Index (NDWI) in order to map glacier lakes based on a local adaptive thresholding method (Li & Sheng 2012). This method was also used by Allen & Pavelsky (2015) to generate a land/water mask for North America using the Modified Normalized Difference Water Index (MNDWI). Rokni *et al.* (2014) modeled the spatio-temporal variations of Urmia Lake over the period 2000–2013. They investigated different satellite-derived spectral indices (NDWI, MNDWI, NDMI (Normalized Difference Moisture Index), AWEI (Automated Water Extraction Index), NDVI (Normalized Difference Vegetation Index), and WRI (Water Ratio Index)) for water extraction. NDWI showed the best results compared with the other indices (Rokni *et al.* 2014). The Weighted Normalized Difference Water Index (WNDWI) is proposed by Guo *et al.* (2017) to reduce errors due to misclassified turbid water, small water bodies, and some land features in a shadow area. This index was tested in China and compared with NDWI, MNDWI, and AWEI. In order to determine the threshold of these indices, three methods including constant value, Otsu's method, and multiple thresholds were used. Results demonstrate that the new index with the threshold of 0 showed the best results.

In this study, Urmia Lake's water area fluctuations are estimated for 5 consecutive years (2013–2017) using six spectral indices that were used most widely in previous studies (NDWI, MNDWI, NDMI, AWEI, WRI, and NDVI). Unlike most studies in this field that use an empirical thresholding method to estimate the threshold value, in this research, Otsu's auto-thresholding method was used. Moreover, a new index was developed to determine more accurate water/salt boundary of the lake.

MATERIALS AND METHODS

Study area

Lake Urmia is located between two provinces (West and East Azerbaijan) in North West of Iran (37° 30′ N, 46° 0′ E). The average depth of the lake is 6 m and the maximum depth is 16 m (Abazopoulos *et al.* 2006). The basin area of the lake is about 51,876 km^2 which is equivalent to more than 3% of the total area of Iran (Eimanifar & Mohebbi 2007). Figure 1 depicts the study area and the Landsat 8 image of Lake Urmia.

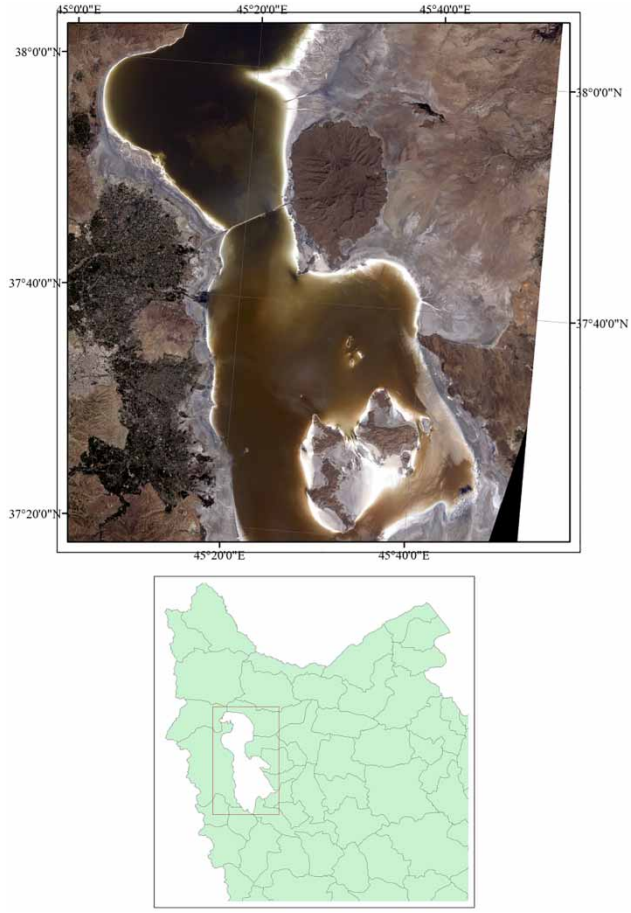

Figure 1 | Location of Lake Urmia in Iran and its Landsat image.

Datasets

In this study, five Landsat 8 images were used. Landsat 8 was launched on 11 February 2013 and acquires images of the whole Earth every 16 days. Landsat 8 images related to Urmia Lake were downloaded from https://earthexplorer.usgs.gov, which were acquired in June from 2013 to 2017. Descriptions regarding images are shown in Table 1.

Methods

The proposed method was applied according to Figure 2. At first, radiometric and geometric corrections and also cloud detection were performed on the Landsat images. Then, spectral indices were extracted from the corrected Landsat 8 images. Water body was obtained from the extracted indices and Otsu's thresholding method. Finally, to assess the

Table 1 | Specification of satellite images used in this study

Dataset	Image name	Date	Path/row
1	LC08_L1TP_169034_20130615_20170503_01_T1	15 June 2013	169/34
2	LC08_L1TP_169034_20140618_20170421_01_T1	18 June 2014	169/34
3	LC08_L1TP_169034_20150621_20170407_01_T1	21 June 2015	169/34
4	LC08_L1TP_169034_20160623_20170323_01_T1	23 June 2016	169/34
5	LC08_L1TP_169034_20170610_20170627_01_T1	10 June 2017	169/34

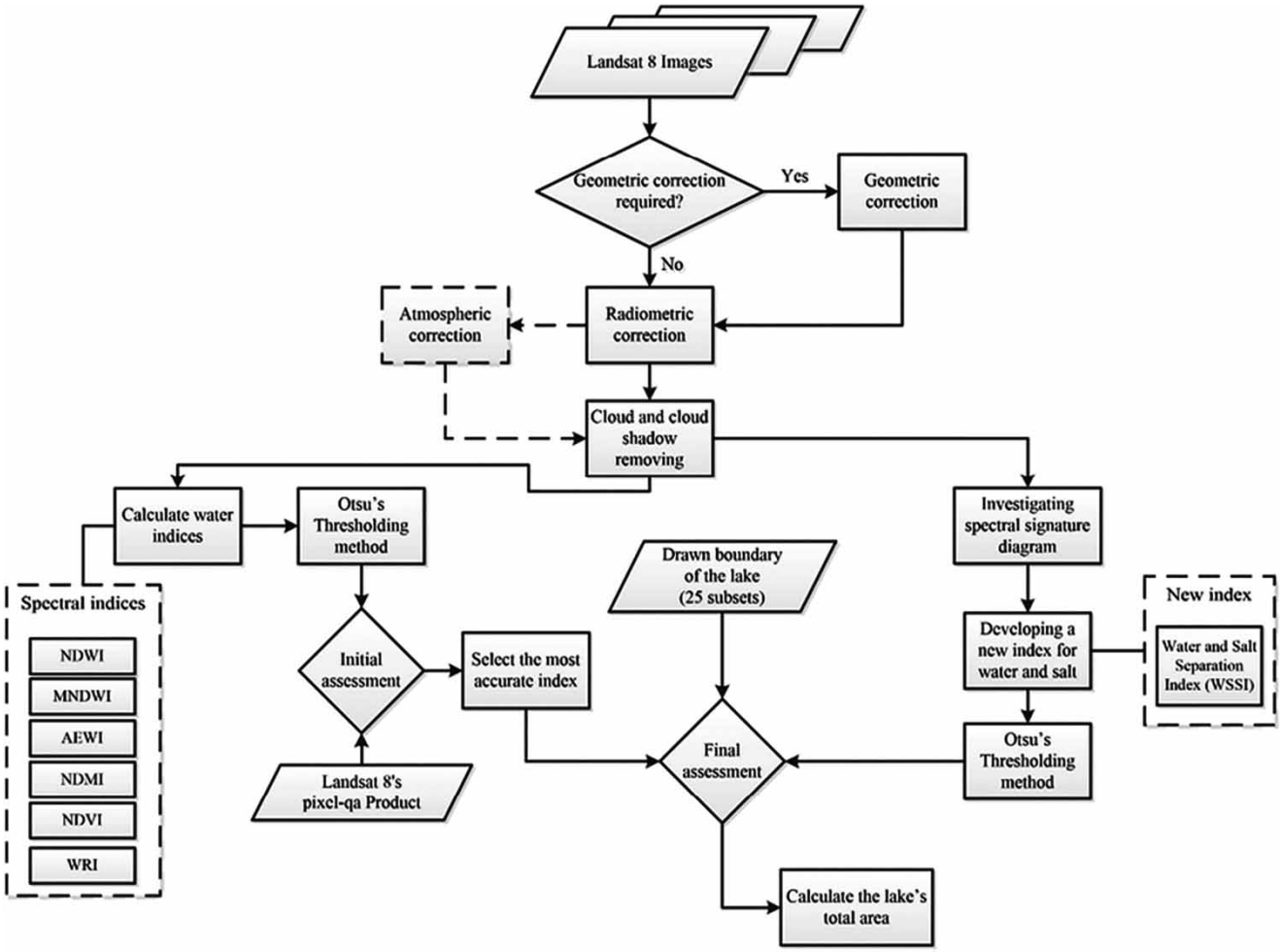

Figure 2 | Flow chart of research study to extract water body.

accuracy of the results of our water extraction method, Landsat pixel QA product, drawn boundary of the lake, and statistical measures were employed.

In the pre-processing step, the geometric correction was performed on images. Then, the radiometric correction was performed using the existing values in the header of images and the related equations (Zanter 2016). In this process, Digital number values are converted into spectral radiance and then the top of atmosphere (TOA) reflectance. The next step is cloud removal from images. Owing to their thickness, shape, altitude, and different distribution, clouds have various effects on the transmission of radiation signals and

also prevent information from the Earth reaching the sensor at the time of image acquisition. Moreover, high-reflectance values of clouds and low-reflectance values of cloud shadow in satellite images will cause many problems in classification and thresholding. In this manner, first, clouds and their shadows were determined using the Function of Mask (Fmask) cloud detection algorithm and other algorithms developed by Kim *et al.* (2013), which used Otsu's thresholding method. Then, a cloud and cloud's shadow mask were created for each image by combining the results of these algorithms and also the quality assessment band, available with Landsat 8 images. Pixels related to these masks removed from images and the values turned to null. To determine the boundary of the lake, six mentioned spectral indices were calculated for each image according to Rokni *et al.* (2014) and Table 2. These are some of the most popular spectral indices that were most used in previous studies.

We found that the above indices worked well in the water bodies where the boundary between water and land immediately changed and detected this boundary with high precision. But in water bodies such as Urmia Lake, which has a salt shore, the mentioned indices do not determine the boundaries of water and salt with sufficient accuracy. For this reason, the Water and Salt Separation Index (WSSI) was extracted from the spectral signature diagram of these features to determine the boundary of water. Figure 3 shows the spectral signature diagram of the three main features including water, salt, and land obtained from Landsat 8 images in this area.

As shown in Figure 3, reflectance values of salt class in bands 3, 4, and 5 of Landsat 8 are higher than the water one.

Table 2 | Spectral indices used for water extraction (Rokni *et al.* 2014)

Index	Equation	References
AWEI	$4 \times (\text{Green} - \text{MIR}) - (0.25 \times \text{NIR} + 2.75 \times \text{SWIR})$	Feyisa *et al.* (2014)
MNDWI	$(\text{Green} - \text{MIR})/(\text{Green} + \text{MIR})$	Xu (2006)
NDMI	$(\text{NIR} - \text{MIR})/(\text{NIR} + \text{MIR})$	Wilson & Sader (2002)
NDVI	$(\text{NIR} - \text{Red})/(\text{NIR} + \text{Red})$	Rouse *et al.* (1974)
NDWI	$(\text{Green–NIR})/(\text{Green} + \text{NIR})$	McFeeters (1996)
WRI	$(\text{Green} + \text{Red})/(\text{NIR} + \text{MIR})$	Shen & Li (2010)

Green, MIR, NIR, SWIR, and Red are green, middle infrared, near-infrared, short-wave infrared, and red bands of the sensor, respectively.

For this reason, the WSSI was proposed based on the mentioned three bands according to the following equation:

$$\text{WSSI} = \frac{\rho 4 - \rho 5}{(\rho 3 + \rho 4)} \quad (1)$$

where ρn is the reflectance (TOA or surface) for the band n of Landsat 8.

Different methods such as spectral indices, classification, and segmentation can be used to extract the water extent from satellite images (Richards & Richards 1999). Use of spectral indices is one of the easiest and most common methods for extracting water from them, but determining a threshold value can be problematic and time-consuming. In order to extract the water body from a water index, it is necessary to determine a threshold that specifies the boundary between water and other features in the image, which is dependent on the condition of the study area. In most studies, the threshold value is determined by a trial-and-error method according to the characteristics of each study area (Ji Zhang & Wylie 2009). In this research, the thresholds are determined automatically by Otsu's thresholding method.

Otsu's thresholding is a method of choosing a global threshold that has been widely used for its simplicity and effectiveness. In this method, it is assumed that an image has two classes, including background and foreground, and it is possible to separate them from each other using an optimal threshold. A gray-level histogram of an image was employed to find the optimal threshold (Otsu 1979). Therefore, this method needs to calculate a gray-level histogram before it runs out. Double-dimensional Otsu's algorithm simultaneously works on the gray-level threshold of each pixel as well as the spatial correlation information in their neighborhood. Thus, this algorithm provides satisfactory segmentation results when used for noisy images (Vala & Baxi 2013).

Otsu's thresholding method finds a threshold value that minimizes within-class weighted variance and also maximizes between-class variance, which is calculated according to the following equation:

$$\sigma_w^2(t) = q_1(t)\sigma_1^2(t) + q_2(t)\sigma_2^2(t) \quad (2)$$

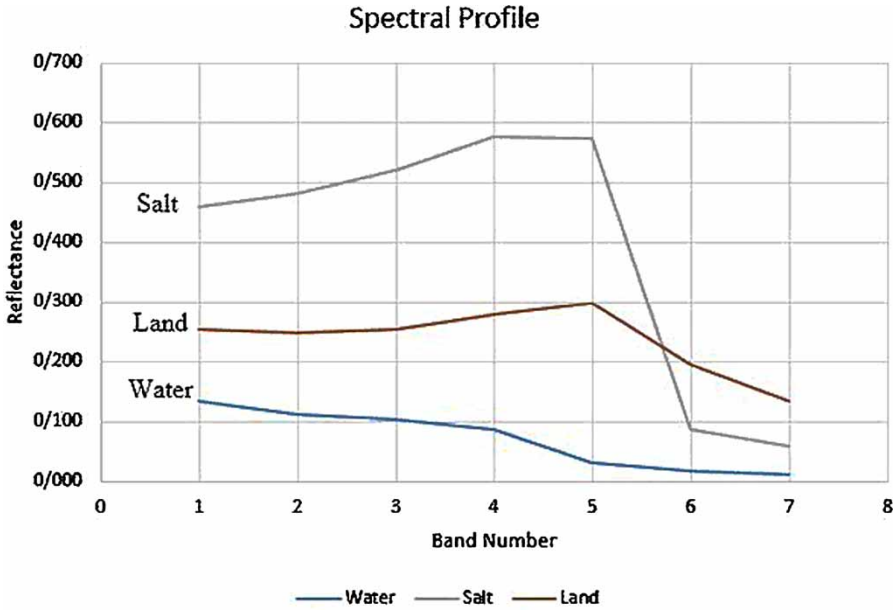

Figure 3 | Spectral signature for the average of water, salt, and drought samples in the Landsat 8 satellite imagery (10 June 2017).

where $\sigma_w^2(t)$ is the weighted variance, q_1 and q_2 are the probability of each class which are calculated as follows:

$$q_1(t) = \sum_{i=1}^{t} p(i) \tag{3}$$

$$q_2(t) = \sum_{i=t+1}^{I} p(i) \tag{4}$$

and the average of each class is calculated using the following equations:

$$\mu_1(t) = \sum_{i=1}^{t} \frac{iP(i)}{q_1(t)} \tag{5}$$

$$\mu_2(t) = \sum_{i=t+1}^{I} \frac{iP(i)}{q_2(t)} \tag{6}$$

and finally, the variance of each class is calculated individually as follows:

$$\sigma_1^2(t) = \sum_{i=1}^{t} [i - \mu_1(t)]^2 \frac{P(i)}{q_1(t)} \tag{7}$$

$$\sigma_2^2(t) = \sum_{i=t+1}^{I} [i - \mu_2(t)]^2 \frac{P(i)}{q_2(t)} \tag{8}$$

Validation

For the initial evaluation of results, the Landsat 8 pixel-qa product was downloaded for each image. This product provides accurate information about cloud, cloud confidence, cloud shadow, snow/ice, and water (landsat surface reflectance quality assessment; available from: https://landsat.usgs.gov/landsat-surface-reflectance-quality-assessment). The C Function of Mask (CFmask) algorithm was used to produce the pixel-qa product, which is a multi-step algorithm that uses a decision tree to label the pixels in the image, and then validates or removes these labels according to the overall statistics of the image (Foga *et al.* 2017). The pixel-qa product for each piece of image data was turned into a binary file containing two classes of water and non-water and was used to provide the region of interest (ROI) and then preliminary evaluation of the results. Finally, the confusion matrix between these six masks and those which were obtained by Otsu's method were calculated.

The confusion matrix was used to evaluate results obtained from this study (Janalipour & Mohammadzadeh 2018). This matrix is usually used to determine the accuracy of the image classification and represents the correspondence between the results of classification and the

reference image. Two basic statistics that can be extracted from this matrix are the overall accuracy (OA) and kappa coefficient (K). OA was calculated according to the following equation:

$$\mathrm{OA} = \frac{\sum_{i=1}^{n} m_{ii}}{N} \tag{9}$$

where OA is the overall accuracy, N is the total number of samples, n is the number of classes, and m_{ii} is the number of samples belonging to class i in the reference map and also in the classification map belonged to the same class. Moreover, K is obtained from the following equation:

$$\mathrm{K} = \frac{N\sum_{i=1}^{n} m_{ii} - \sum_{i=1}^{n} G_i C_i}{N^2 - \sum_{i=1}^{n} G_i C_i} \tag{10}$$

where K is Kappa coefficient, C_i is the number of samples assigned to class i, and G_i is the number of ground truth samples in class i.

RESULTS AND DISCUSSION

In this study, by using Otsu's thresholding method, binary maps regarding water and non-water classes were obtained from all indices. Two examples of these binary maps associated with the dataset 1 are shown in Figure 4, which were obtained from the NDWI and the MNDWI. This figure shows that the outcome of the MNDWI detects more water areas with respect to the NDWI. Moreover, some noise water pixels were observed in the MNDWI result. As can be seen in this figure, results obtained from these two indices are different from each other, especially on the boundary between water and salt. It shows that the main uncertainty and difference in the results' indices may occur in the edge of two regions.

For an initial evaluation, water body extracted from six indices for five images and Otsu's method were evaluated using Landsat 8's pixel-qa product. Landsat 8's pixel-qa product provides a land cover map, which was obtained from Landsat 8 images. It is possible to extract water and non-water classes from pixel-qa and use them for initial evaluation. Using classes obtained from the pixel-qa product and results extracted from spectral indices, a confusion matrix can generate. OA and K extracted from the confusion matrix are presented in Table 3.

In dataset 1, water and non-water classes were extracted from WRI, NDVI, NDMI, MNDWI, AWEI, NDWI, and WSSI, respectively, with OAs of 61.09%, 43.72%, 86.72%, 94.55%, 93.95%, 99.20%, and 98.15%. According to this result, it seems that NDWI and WSSI are more successful than other ones in the mentioned task. Furthermore, outcomes

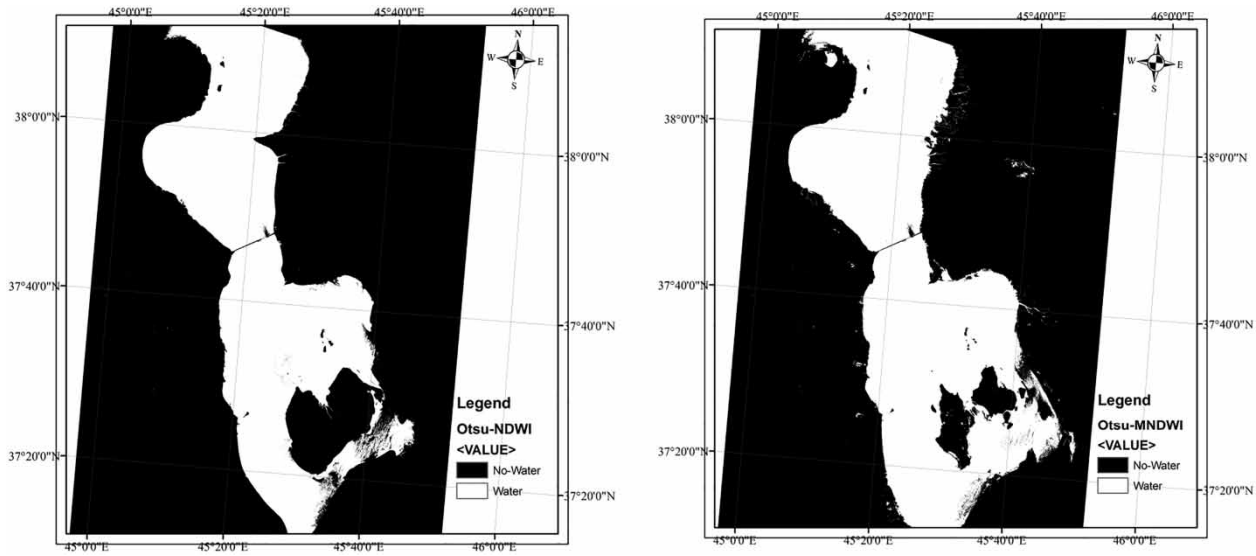

Figure 4 | Binary maps obtained from Otsu's method for the NDWI and the MNDWI in dataset 1 (15 June 2013).

Table 3 | Initial accuracy assessment of spectral indices and Otsu's method using the Landsat 8 pixel-qa product

		Otsu				Otsu	
	Index	OA (%)	K		Index	OA (%)	K
Dataset 1 (15 June 2013)	WRI	61.09	0.31	Dataset 2 (18 June 2014)	WRI	53.88	0.19
	NDVI	43.72	0.14		NDVI	32.36	0.07
	NDMI	86.72	0.67		NDMI	84.33	0.54
	MNDWI	94.55	0.85		MNDWI	89.16	0.65
	AWEI	93.95	0.84		AWEI	88.51	0.61
	NDWI	99.20	0.98		NDWI	97.72	0.91
	WSSI	98.15	0.95		WSSI	96.19	0.86
Dataset 3 (21 June 2015)	WRI	55.11	0.19	Dataset 4 (23 June 2016)	WRI	66.51	0.37
	NDVI	30.74	0.06		NDVI	42.85	0.14
	NDMI	80.55	0.29		NDMI	85.50	0.63
	MNDWI	88.93	0.63		MNDWI	93.64	0.83
	AWEI	86.60	0.51		AWEI	93.45	0.81
	NDWI	97.61	0.90		NDWI	97.99	0.94
	WSSI	96.50	0.86		WSSI	96.96	0.92
Dataset 5 (10 June 2017)	WRI	65.35	0.36				
	NDVI	43.04	0.14				
	NDMI	87.08	0.65				
	MNDWI	95.35	0.87				
	AWEI	91.52	0.76				
	NDWI	99.03	0.97				
	WSSI	98.75	0.96				

of WRI, NDVI, and NDMI are not robust enough for water extraction. Moreover, results of OA of NDWI and MNDWI are confirmed in Figure 4. Furthermore, values of OA and K in the NDWI and the WSSI were near to each other, which is not observed in other indices. This indicates that results of the two mentioned indices were more robust than others.

As shown in Table 3, water and non-water classes obtained from the NDVI with the maximum OA of 43.72% are not accurate. This shows that the vegetation index is not appropriate for separating water and non-water from each other. In classification results, NDWI and Otsu's thresholding with the minimum OA of 97.61% have the best outcome. Moreover, results of WSSI, MNDWI, AWEI, NMDI, and WRI are also acceptable and accurate.

In order to assess results in a schematic manner, binary maps generated by these indices for the 2017 image are shown in Figure 5. It is clear that the NDVI has detected many non-water objects around the lake erroneously in the water class, so the Otsu's thresholding is not a suitable method to determine the threshold of water and land in this index. From this result, it is concluded that an appropriate feature space can be used to extract water body from Otsu's thresholding. Moreover, the NDWI seems to be an appropriate feature for detecting water.

As mentioned, the Landsat 8 pixel-qa product was produced from an automatic image processing algorithm. Therefore, it may have some errors and uncertainty. For this reason, in the final evaluation of the results, five subsets of each image were selected randomly. The location of these subsets is shown in Figure 6. Then, using the various band combinations of Landsat 8 images as well as high-resolution images from Google Earth, the precise boundary of the lake water was drawn in each of these subsets. Using the precise boundary and results of NDWI and WSSI, the final accuracy assessment was done.

OA and K of NDWI and WSSI obtained from the drawn boundary are presented in Tables 4–8. According to these tables, the WSSI is more successful than the NDWI in separating water and non-water classes. In most cases, the WSSI improves OA more than 1% with respect to the NDWI. There are two main points. In the first point, it seems the use of a spectral index that can consider saline and water areas together is better than a water index in our study area. Moreover, since there were many test

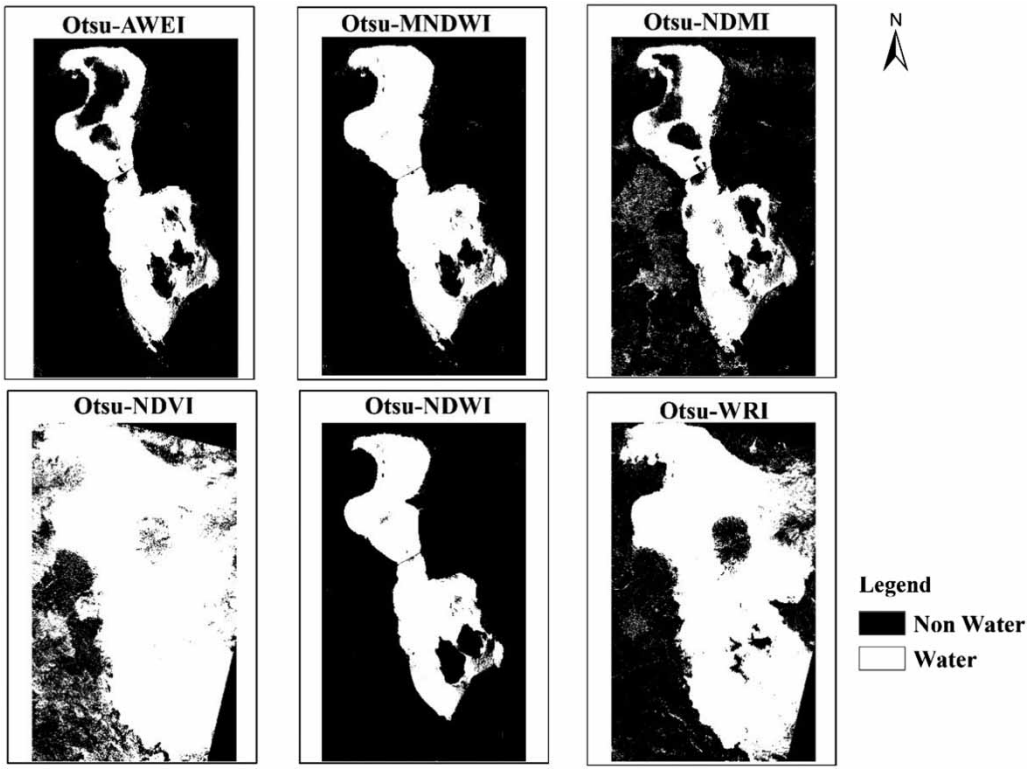

Figure 5 | Water masks obtained by Otsu's method from six spectral indices in dataset 5 (10 June 2017).

pixels, an improvement of 1% in OA was a good achievement. In S1 of dataset 1, OA and K of the WSSI were equivalent to 99.41% and 0.99, respectively. This result confirms the outcomes of Table 3 and showed that the WSSI was robust for water extraction.

In S1, S2, S4, and S5 of dataset 1, OA of the WSSI was greater than the NDWI. Moreover, based on OA, the WSSI outperforms the NDWI in all subsets of datasets 2 and 3. Also, in S1, S4, and S5 of dataset 4, it seems that the WSSI was more robust than the NDWI for water extraction. Finally, similar to dataset 1, the WSSI was more successful than the NDWI in S1, S2, S4, and S5. According to these results, the accuracy of WSSI in water extraction over 21 subsets from 25 was better than the NDWI. Therefore, it can be concluded that the WSSI was more robust than the NDWI.

In order to assess outcomes schematically, drawn ROI, Landsat 8 pixel-qa product, NDWI, and WSSI results are shown in Figure 7. According to these figures, the Landsat 8 pixel-qa product cannot detect water body around the salt area and it seems that the drawn ROI was more robust for accuracy assessment. The visual analysis showed that the WSSI was more successful than the NDWI for detecting water body.

In order to illustrate results, areas obtained from the drawn areas, Otsu-NDWI and Otsu-WSSI, are shown in Tables 9–13. Areas of S1 in datasets 1–5 are, respectively, equal to 222.5, 188.9, 186.2, 225, and 219 km^2. In general, it seems that the obtained area from the Otsu-WSSI was more similar than the NDWI to the drawn area. Areas obtained from the WSSI were closer than the NDWI to the drawn area. According to the results, it seems that the area of Lake Urmia was decreased in 2014 and 2015 with respect to 2013.

In general, it can be concluded that the NDWI in almost all cases underestimates the area of the lake, but the WSSI estimations were much closer to real values. The values in the tables indicate that in almost all 25 subsets, the WSSI derived better results. In most images, subset 3 showed a considerable difference (more than 15 km^2) for both indices compared with real values. This is because this subset was located in a part of the lake where there was no clear boundary between water and salt in the images. Hence, it was difficult to detect the boundary of water as a reference

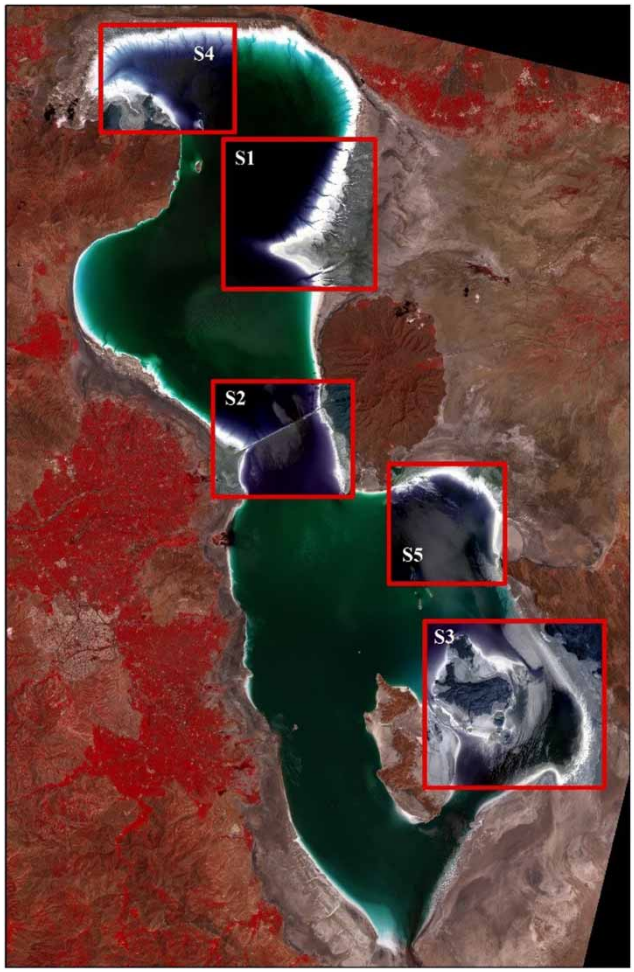

Figure 6 | Location of random subsets on the lake.

Table 4 | Results of the evaluation of the new water index and the NDWI with the drawn boundary for the first dataset

		Otsu-NDWI		Otsu-WSSI	
	Subset	OA (%)	K	OA (%)	K
Dataset 1 (15 June 2013)	S1	99.06	0.98	99.41	0.99
	S2	98.66	0.97	99.36	0.98
	S3	93.97	0.85	90.11	0.80
	S4	98.95	0.98	99.21	0.98
	S5	97.17	0.92	98.91	0.97

map in this subset, so these values cannot be considered as a defect in these indices.

The total area of the lake obtained from both indices in these 5 years is shown in Table 14. Comparing the results of Otsu-NDWI and Otsu-WSSI indicates that there was the largest difference (about 175.7 km^2) in 2016 and the least difference (about 45 km^2) in 2017 between the estimated areas by these indices. In general,

Table 5 | Results of the evaluation of the new water index and the NDWI with the drawn boundary for the second dataset

		Otsu-NDWI		Otsu-WSSI	
	Subset	OA (%)	K	OA (%)	K
Dataset 2 (18 June 2014)	S1	99.26	0.98	99.52	0.99
	S2	97.19	0.94	99.02	0.98
	S3	95.64	0.55	97.28	0.77
	S4	96.67	0.93	98.46	0.97
	S5	95.04	0.88	96.67	0.92

Table 6 | Results of the evaluation of the new water index and the NDWI with the drawn boundary for the third dataset

		Otsu-NDWI		Otsu-WSSI	
	Subset	OA (%)	K	OA (%)	K
Dataset 3 (21 June 2015)	S1	98.85	0.98	99.21	0.98
	S2	97.80	0.96	99.01	0.98
	S3	99.37	0.74	99.81	0.94
	S4	96.52	0.93	98.23	0.96
	S5	90.99	0.82	97.12	0.94

Table 7 | Results of the evaluation of the new water index and the NDWI with the drawn boundary for the fourth dataset

		Otsu-NDWI		Otsu-WSSI	
	Subset	OA (%)	K	OA (%)	K
Dataset 4 (23 June 2016)	S1	88.55	0.77	91.93	0.83
	S2	98.90	0.97	98.85	0.97
	S3	89.00	0.68	83.39	0.58
	S4	96.05	0.91	97.39	0.94
	S5	96.52	0.90	96.58	0.90

Table 8 | Results of the evaluation of the new water index and the NDWI with the drawn boundary for the fifth dataset

		Otsu-NDWI		Otsu-WSSI	
	Subset	OA (%)	K	OA (%)	K
Dataset 5 (23 June 2016)	S1	98.52	0.97	99.12	0.98
	S2	98.16	0.96	99.27	0.98
	S3	91.46	0.79	91.14	0.79
	S4	96.56	0.93	97.99	0.96
	S5	93.74	0.85	95.02	0.88

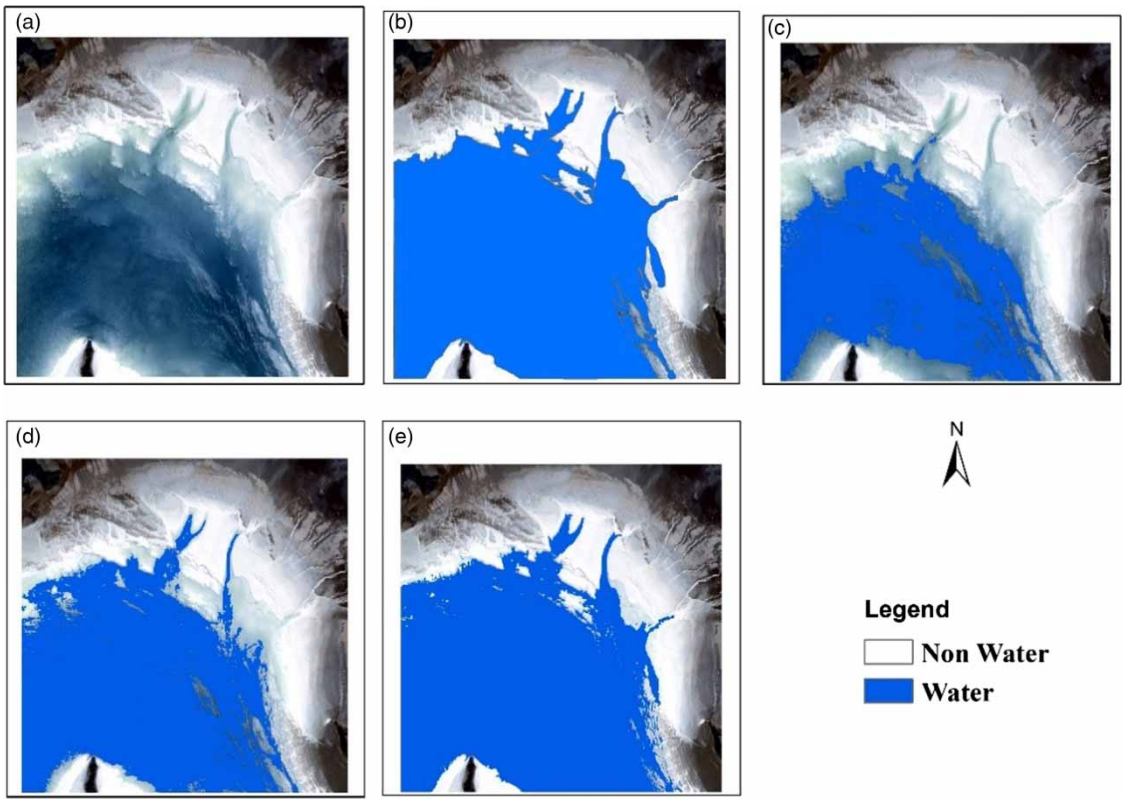

Figure 7 | Comparing water extent in (a) Landsat 8 true-color image, (b) drawn ROI, (c) Landsat 8's pixel-qa product, (d) Otsu-NDWI, and (e) Otsu-WSSI.

Table 9 | Area comparison of the Otsu-NDWI and the Otsu-WSSI in dataset 1

	Subset	Drawn area (km^2)	Otsu-NDWI area (km^2)	Otsu-WSSI area (km^2)	Otsu-NDWI–drawn area	Otsu-WSSI–drawn area
Dataset 1 (15 June 2013)	S1	222.550	220.316	222.180	−2.234	−0.37
	S2	177.403	175.444	177.954	−1.959	0.551
	S3	156.337	124.868	185.335	−31.469	28.998
	S4	155.982	154.379	155.763	−1.603	−0.219
	S5	165.584	159.946	164.475	−5.638	−1.109

Table 10 | Area comparison of the Otsu-NDWI and the Otsu-WSSI in dataset 2

	Subset	Drawn area (km^2)	Otsu-NDWI area (km^2)	Otsu-WSSI area (km^2)	Otsu-NDWI–drawn area	Otsu-WSSI–drawn area
Dataset 2 (18 June 2014)	S1	188.955	178.015	189.550	−10.94	0.595
	S2	145.604	139.560	147.001	−6.044	1.397
	S3	32.615	15.468	27.980	−17.147	−4.635
	S4	103.896	97.784	102.758	−6.112	−1.138
	S5	68.866	65.221	72.823	−3.645	3.957

for most years, there was a considerable difference (more than 100 km^2) between the total areas of the lake. A great difference between areas obtained from WSSI and NDWI was observed, although there was a little difference among OA of them. Since the results of the Otsu-WSSI are more robust than the Otsu-NDWI, it can be concluded that the total estimated area of the lake by this index was closer to the ground truth.

Table 11 | Area comparison of the Otsu-NDWI and the Otsu-WSSI in dataset 3

	Subset	Drawn area (km^2)	Otsu-NDWI area (km^2)	Otsu-WSSI area (km^2)	Otsu-NDWI–drawn area	Otsu-WSSI–drawn area
Dataset 3 (21 June 2015)	S1	186.299	183.588	186.860	−2.711	0.561
	S2	132.289	127.825	133.078	−4.464	0.789
	S3	7.3460	4.428	7.096	−2.918	−0.25
	S4	104.377	97.883	102.835	−6.494	−1.542
	S5	107.032	88.801	106.628	−18.231	−0.404

Table 12 | Area comparison of the Otsu-NDWI and the Otsu-WSSI in dataset 4

	Subset	Drawn area (km^2)	Otsu-NDWI area (km^2)	Otsu-WSSI area (km^2)	Otsu-NDWI–drawn area	Otsu-WSSI–drawn area
Dataset 4 (23 June 2016)	S1	225.065	184.284	197.889	−40.781	−27.176
	S2	183.723	183.936	185.962	0.213	2.239
	S3	83.291	124.964	159.249	41.673	75.958
	S4	151.672	174.296	152.493	22.624	0.821
	S5	166.253	168.077	172.342	1.824	6.089

Table 13 | Area comparison of Otsu-NDWI and Otsu-WSSI in dataset 5

	Subset	Drawn area (km^2)	Otsu-NDWI area (km^2)	Otsu-WSSI area (km^2)	Otsu-NDWI–drawn area	Otsu-WSSI–drawn area
Dataset 5 (10 June 2017)	S1	219.747	215.230	217.704	−4.517	−2.043
	S2	180.413	176.945	180.391	−3.468	−0.022
	S3	121.425	147.423	153.670	25.998	32.245
	S4	145.733	138.547	141.943	−7.186	−3.79
	S5	151.803	154.541	161.273	2.738	9.47

Table 14 | Total area of Urmia Lake derived from the Otsu-NDWI and the Otsu-WSSI

Year	Otsu-NDWI area (km^2)	Otsu-WSSI area (km^2)	Otsu-WSSI–Otsu-NDWI
2013	2438.22	2549.23	111/01
2014	1670.23	1817.75	147/51
2015	1561.07	1676.29	115/22
2016	2401.38	2577.03	175/64
2017	2474.05	2519.17	45/11

CONCLUSION

In this study, to determine the exact area of Lake Urmia in different years and to determine the exact boundary between water, land, and salt around the lake, different spectral indices, such as NDWI, MNDWI, NDVI, WRI, NDMI, and AWEI, were extracted on the lake using Landsat 8 satellite images. Then, by using Otsu's thresholding method, a threshold value was automatically determined to detect the boundary of the lake. Among these spectral indices, the Otsu-NDWI showed the best results both visually and in comparison with the Landsat 8's Pixel-qa product. However, it underestimated the area of the lake in almost all images. Therefore, in order to better estimate the lake area and determine the exact boundary between water and salt around it, according to the spectral signature diagram of water, salt, and land, a new index called the WSSI was developed. The results showed that the WSSI provides a better estimation of the lake area with respect to the NDWI. It is suggested that in the future studies, this index will be tested in other study areas for better verification. Moreover, other sensors can be employed to test the efficiency of the proposed index. A huge change in water area may result in climate change; therefore, the proposed method can be utilized for the mentioned studies.

ACKNOWLEDGEMENTS

We would like to show our gratitude to 'U.S. Geological Survey (USGS)/NASA Landsat program' for providing the Landsat data and its useful products.

REFERENCES

Abatzopoulos, T. J., Baxevanis, A. D., Triantaphyllidis, G. V., Criel, G., Pador, E. L., Van Stappen, G. & Sorgeloos, P. 2006 Quality evaluation of Artemia urmiana Günther (Urmia Lake, Iran) with special emphasis on its particular cyst characteristics (International Study on Artemia LXIX). *Aquaculture* **254** (1–4), 442–454.

Abazopoulos, T. J., Agh, N., Van Stappen, G., Razavi Rouhani, S. M. & Sorgeloos, P. 2006 Artemia sites in Iran. *Journal of the Marine Biological Association* **86**, 299–307.

Acharya, T. D., Subedi, A., Yang, I. T. & Lee, D. H. 2017 Combining water indices for water and background threshold in Landsat image. *Paper Read at Multidisciplinary Digital Publishing Institute Proceedings*.

Allen, G. H. & Pavelsky, T. M. 2015 Patterns of river width and surface area revealed by the satellite-derived North American river width data set. *Geophysical Research Letters* **42** (2), 395–402.

Eimanifar, A. & Mohebbi, F. 2007 Urmia Lake (northwest Iran): a brief review. *Saline Systems* **3** (1), 1–8.

Feyisa, G. L., Meilby, H., Fensholt, R. & Proud, S. R. 2014 Automated Water Extraction Index: a new technique for surface water mapping using Landsat imagery. *Remote Sensing of Environment* **140**, 23–35.

Foga, S., Scaramuzza, P. L., Guo, S., Zhu, Z., Dilley, R. D., Beckmann, T., Schmidt, G. L., Dwyer, J. L., Joseph Hughes, M. & Laue, B. 2017 Cloud detection algorithm comparison and validation for operational Landsat data products. *Remote Sensing of Environment* **194**, 379–390.

Guo, Q., Pu, R., Li, J. & Cheng, J. 2017 A weighted normalized difference water index for water extraction using Landsat imagery. *International Journal of Remote Sensing* **38** (19), 5430–5445.

Huang, C., Chen, Y., Zhang, S. & Wu, J. 2018 Detecting, extracting, and monitoring surface water from space using optical sensors: a review. *Reviews of Geophysics* **56** (2), 333–360.

Huovinen, P., Ramírez, J., Caputo, L. & Gómez, I. 2019 Mapping of spatial and temporal variation of water characteristics through satellite remote sensing in Lake Panguipulli, Chile. *Science of the Total Environment* **679**, 196–208.

Janalipour, M. & Mohammadzadeh, A. 2018 Evaluation of effectiveness of three fuzzy systems and three texture extraction methods for building damage detection from post-event LiDAR data. *International Journal of Digital Earth* **11** (12), 1241–1268.

Ji, L., Zhang, L. & Wylie, B. 2009 Analysis of dynamic thresholds for the normalized difference water index. *Photogrammetric Engineering & Remote Sensing* **75** (11), 1307–1317.

Kim, B., Han, Y., Kim, Y. & Kim, Y. 2013 Generation of cloud-free imagery using Landsat-8. In: *Paper SC02-0828 in the 34th Asian Conference on Remote Sensing, Proceedings, ACRS*, pp. 20–24.

Li, J. & Sheng, Y. 2012 An automated scheme for glacial lake dynamics mapping using Landsat imagery and digital elevation models: a case study in the Himalayas. *International Journal of Remote Sensing* **33** (16), 5194–5213.

McFeeters, S. K. 1996 The use of the normalized difference water index (NDWI) in the delineation of open water features. *International Journal of Remote Sensing* **17** (7), 1425–1432.

Mohebzadeh, H. & Fallah, M. 2019 Quantitative analysis of water balance components in Lake Urmia, Iran using remote sensing technology. *Remote Sensing Applications: Society and Environment* **13**, 389–400.

Otsu, N. 1979 A threshold selection method from gray-level histograms. *IEEE Transactions on Systems, Man, and Cybernetics* **9** (1), 62–66.

Maleki, R., Nooripoor, M., Azadi, H. & Lebailly, P. 2018 Vulnerability assessment of rural households to Urmia Lake drying (the case of Shabestar region). *Sustainability* **10** (6), 1862.

Richards, J. A. & Richards, J. A. 1999 *Remote Sensing Digital Image Analysis*. Vol. 3. Springer, Berlin.

Rokni, K., Ahmad, A., Selamat, A. & Hazini, S. 2014 Water feature extraction and change detection using multitemporal Landsat imagery. *Remote Sensing* **6** (5), 4173–4189.

Rouse Jr., J. W., Haas, R. H., Schell, J. A. & Deering, D. W. 1974 'Monitoring vegetation systems in the Great Plains with ERTS. 3rd ERTS Symp, NASA SP-351, Vol. 1, U.S. Gov. printing office, Washington, DC, pp. 309–317.

Shen, L. & Li, C. 2010 Water body extraction from Landsat ETM+ imagery using adaboost algorithm. In: *2010 18th International Conference on Geoinformatics*.

Vala, M. H. J. & Baxi, A. 2013 A review on Otsu image segmentation algorithm. *International Journal of Advanced Research in Computer Engineering & Technology (IJARCET)* **2** (2), 387–389.

Wilson, E. H. & Sader, S. A. 2002 Detection of forest harvest type using multiple dates of Landsat TM imagery. *Remote Sensing of Environment* **80** (3), 385–396.

Xu, H. 2006 Modification of normalised difference water index (NDWI) to enhance open water features in remotely sensed imagery. *International Journal of Remote Sensing* **27** (14), 3025–3033.

Zanter, K. 2016 *Landsat 8 (L8) Data Users Handbook*. Landsat Science Official Website. Available from: https://landsat.usgs.gov/landsat-8-l8-data-users-handbook (accessed 20 January 2018).

First received 16 April 2019; accepted in revised form 4 November 2019. Available online 17 December 2019